SCIENTIFIC REPORTS

OPEN

SUBJECT AREAS:
SOLAR CELLS
SOLID-STATE CHEMISTRY
APPLIED PHYSICS
ELECTRONIC STRUCTURE

Received
1 November 2012

Accepted
29 January 2013

Published
15 February 2013

Correspondence and requests for materials should be addressed to F.Q.H. (huangfq@mail.sic.ac.cn)

Observation of an Intermediate Band in Sn-doped Chalcopyrites with Wide-spectrum Solar Response

Chongyin Yang[1,2], Mingsheng Qin[1], Yaoming Wang[1], Dongyun Wan[1], Fuqiang Huang[1,2] & Jianhua Lin[2]

[1]CAS Key Laboratory of Materials for Energy Conversion, Shanghai Institute of Ceramics, Chinese Academy of Sciences, Shanghai 200050, P. R. China, [2]Beijing National Laboratory for Molecular Sciences and State Key Laboratory of Rare Earth Materials Chemistry and Applications, College of Chemistry and Molecular Engineering, Peking University, Beijing 100871, P. R. China.

Nanostrcutured particles and polycrystalline thin films of Sn-doped chalcopyrite are synthesized by newly-developed methods. Surprisingly, Sn doping introduces a narrow partially filled intermediate band (IB) located ~1.7 eV ($CuGaS_2$) and ~0.8 eV ($CuInS_2$) above the valance band maximum in the forbidden band gap. Diffuse reflection spectra and photoluminescence spectra reveal extra absorption and emission spectra induced by the IBs, which are further supported by first-principle calculations. Wide spectrum solar response greatly enhances photocatalysis, photovoltaics, and photo-induced hydrogen production due to the intermediate band.

The inability to capture photon energy lower than the band gap of the light absorber poses a fundamental limit to the theoretical efficiency of photovoltaic (PV) cells[1]. Although solar cells consisting of multiple absorber layers with different band gaps can mitigate this problem, and such strategy is indeed implemented in some III–V based solar cells[2], the increased complexity inevitably increases the cost of the cells. Alternatively, solar cells with an intermediate band (IB) promise to extend the absorption spectrum while at the same time preserve the output voltage. The theoretical efficiency (η) of intermediate band cells can reach 63%, far beyond the single-junction silicon solar cells ($\eta \leq 31\%$)[3]. Band diagram of the IB cells is shown in Fig. 1. The partially-filled intermediate band can provide empty states to receive the electrons pumped by photon "3" and further pump the electrons from there by photon "2". The solar response is significantly extended to lower energy photons, especially in near-infrared (NIR) region. As well known, the solar spectrum (on earth) is a blackbody radiation with strong visible and NIR emissions. In consequence, the multi-photon absorption of two sub-band gaps (E_H and E_L) efficaciously enhances the photocurrent without photo-voltage degradation.

The intermediate band material of N-doped GaAs was estimated to achieve $\eta \sim 40\%$ in a multiband cell[4], but the III–V thin films are fabricated by expensive metal organic chemical vapor deposition, which is not affordable for civilian uses. Cu-based chalcopyrite semiconductors are nowadays used as light absorbers in the highest efficiency thin-film solar cells ($Cu(In,Ga)(Se,S)_2$, $\eta = 20.3\%$)[5,6]. The solar cells possess an extraordinary defect tolerance and the possibility for economic applications. Due to the band gaps deviated from 2.4 eV for $CuGaS_2$ (CGS) to 1.45 eV for $CuInS_2$ (CIS), they only absorb partial solar spectrum. Thus, intermediate bands introduced to these chalcopyrites should enable them to more efficiently utilize solar energy.

Many predictions have been theoretically placed on the wide-spectrum absorption of chalcopyrites by introducing various dopants (Ti, V, Cr, Ni, etc.)[7–11], but direct experimental evidences on the existence of intermediate band were still lack[12,13]. For example, the 3*d*-metal atoms commonly doped in $CuGaS_2$ form IBs in the forbidden band gap from these 3*d*-metal orbitals[7–9]. Since the 3*d* states of transition metal are rather localized, the optical transitions related to IB may not be favorable due to indirect transition or low light absorption coefficients. Furthermore, the low carrier mobility on the 3*d* orbitals of transition metal cannot satisfy the requirement of photovoltaic cells. Thus, the transition metal might not be the best candidate to achieve high efficiently IB absorption in chalcopyrite.

In this paper, intermediate bands were introduced into $CuMS_2$ (M = In, Ga) by Sn doping (Fig. 1) to greatly enhance solar energy absorption and conversion. Nanostrcutured Sn-doped $CuMS_2$ powder was synthesized by simple mechanically ball-milling of Cu_2S and M_2S_3, and the corresponding thin films were prepared by a non-vacuum solution-based approach. The intermediate band in Sn-doped $CuMS_2$ was directly evidenced by diffuse reflection spectra and photoluminescence spectra. With the aid of wide-spectrum solar response, especially from

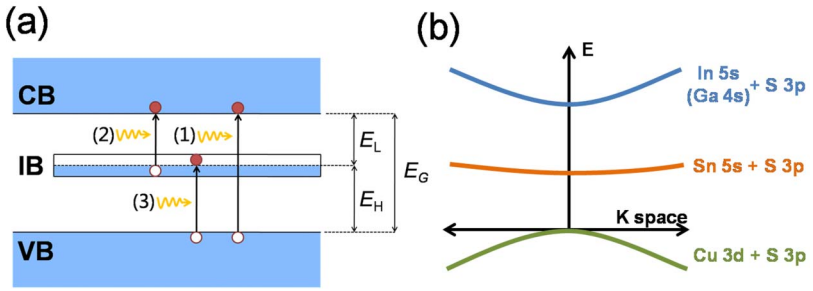

Figure 1 | A proposed scheme of intermediate band in Sn-doped Chalcopyrites. (a) Band diagram of an intermediate band solar cell, showing the bandgap (E_g), the sub-bandgaps (E_H, E_L) and the CB, IB and VB. "(1)", "(2)" and "(3)" represent photon absorptions. (b) Band structure of Sn-doped CuMS_2 (M = In, Ga).

the NIR region, the more efficient solar energy conversions were yielded in photocatalytic reactions and photoelectrochemical cells.

Results

In order to evaluate the ball-milling method, the harvested CuMS_2 (M = In, Ga) powders were investigated by transmission electron microscopy (TEM) (Fig. 2a). The morphologies of $CuIn_{1-x}Ga_xS_2$ are fairly uniform in size of 100–200 nm. STEM elemental mapping analysis was further examined the distribution of Sn in the doped samples. The elemental mappings of Ga, Sn, and S, as shown in Fig. 2b, have a homogeneous spatial distribution. The uniform elemental distribution of $CuIn_{1-x}Sn_xS_2$ was also confirmed (see in Fig. S1 of Supporting Information). The concentration of Sn was investigated by quantitative analyses of energy-dispersive X-ray spectroscopy (EDS). The EDS measurements are in good agreement with the nominal values, as summarized in Table S1 of Supporting Information.

The phase purity of Sn-doped CuMS_2 (M = In, Ga) was investigated by X-ray diffraction (XRD). The diffraction peaks were all indexed to a chalcopyrite structure (Fig. 2c)[14], and no impurities were observed. Linear dependence of lattice constants (a, c) on the Sn-doping level (x) for $CuM_{1-x}Sn_xS_2$ reveals the typical feature of solid solution, as shown in Fig. 2d. The successful doping of Sn is also evidenced by a right shift of XRD peaks in $CuIn_{1-x}Sn_xS_2$ and a left shift in $CuGa_{1-x}Sn_xS_2$ due to the atom radius of Sn (1.41 Å) smaller than In (1.44 Å) and larger than Ga (1.26 Å).

From the above results and discussion, the ball milling is demonstrated to be an excellent method to synthesize uniform nanostructured CuMS_2 powder. Quantitative composition analysis and crystal structure evolution reveal that the as-prepared samples possess both the homogeneity of element distributions and the compatibility of lattice structure. High quality of samples is due to selecting Cu_2S and M_2S_3 as "*metastable*" starting materials[15]. The mechanic energy from ball-milling initializes the exothermic reaction of Cu_2S and M_2S_3 to

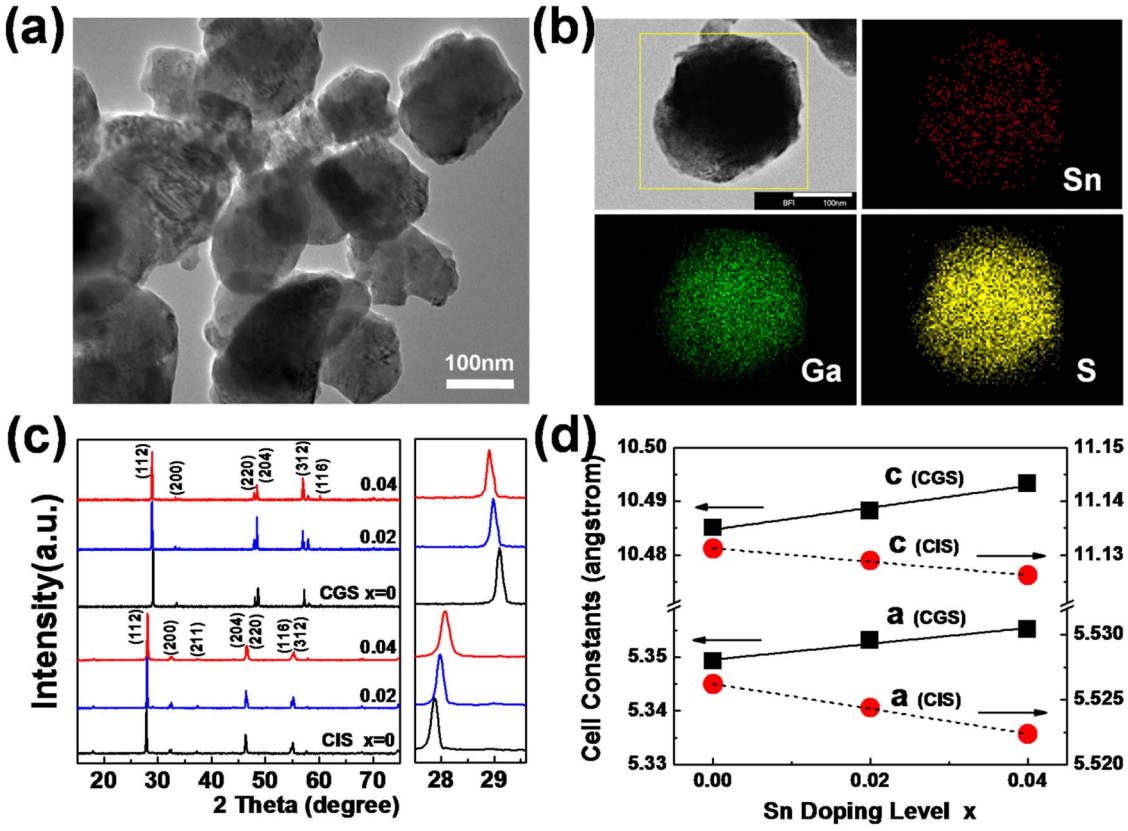

Figure 2 | Analyses of as-prepared $CuGa_{0.96}Sn_{0.04}S_2$ particles. (a) TEM, (b) STEM and elemental mapping of Cu. (c) XRD powder patterns of $CuIn_{1-x}Sn_xS_2$ (CIS) and $CuGa_{1-x}Sn_xS_2$ (CGS); the right: (112) peak shift. (d) Linear dependence of cell constants (a, c) on x for $CuM_{1-x}Sn_xS_2$.

rapidly form $CuMS_2$. Similarly, ceramic $CuInSe_2$ was sintered by us from the reaction of Cu_2Se and In_2Se_3 at 550°C[16], whose sintering temperature is lower than the reported samples (~700°C)[17]. The polycrystalline $CuIn_{0.7}Ga_{0.3}Se_2$ films were also prepared from Se-coated Cu(Ga) and In layers at 550°C in a few seconds[18]. The proposed method can avoids introducing some potential impurities, which is difficult for solution process methods[19,20]. This newly-developed method is applicable to synthesize the other chalcopyrites.

As shown in Fig. 3a, the color of the pressed $CuGa_{1-x}Sn_xS_2$ powder varies from orange ($x = 0$), dark red ($x = 0.02$), to dark brown ($x = 0.04$). The light absorptions of these powders were verified by UV-Vis-NIR diffuse reflection spectra. The plots of $(\alpha h\nu)^2$ versus $h\nu$ are shown in Fig. 3b and S2a, based on the modified Kubelka–Munk function of $F(R) = (1-R)^2/(2R) = \alpha/S$, where R is the reflectance, and α and S are the absorption and scattering coefficients. With increasing x, the onset of the absorption coefficient shifts significantly to lower photon energy, which is indexed by the direct band gap (E_g) from the extrapolated intercept of the linear portion of the plot of $(\alpha h\nu)^2$ against $h\nu$ (Fig. 3b and S2b). The corresponding band gaps of $CuGa_{1-x}Sn_xS_2$ are 2.35 eV ($x = 0$), 1.98 eV ($x = 0.02$), and 1.80 eV ($x = 0.04$); the E_g of $CuIn_{1-x}Sn_xS_2$ are 1.42 eV ($x = 0$), 1.14 eV ($x = 0.02$), and 1.03 eV ($x = 0.04$). It indicates that Sn doping in $CuMS_2$ successfully extends their solar response spectra (Fig. 3d). In order to show the detail of the absorption spectra, the low absorption coefficient part of $CuGa_{1-x}Sn_xS_2$ are magnified and shown in Fig. 3c. The extra absorption peaks at 0.7 eV and 1.7 eV are related to the absorption extra photons of $h\nu_2$ (IB → CBM, >0.7 eV) and $h\nu_3$ (VBM → IB, >1.7 eV). The similar extra absorption spectra were predicted or observed in other intermediate band related materials (In_2S_3:V, ZnTe:O etc.)[30,31].

In order to meet the requirements for the future applications on thin film photovoltaic cells, the $CuIn_{1-x}Sn_xS_2$ films were prepared by a non-vacuum method and annealed in 5 mol% H_2S-contained Ar atmosphere at 600°C for 15 min. The film is polycrystalline and the average grain size is about 1 μm (Fig. S5), comparable to the $CuInGaSe_2$ (CIGS) film in CIGS solar cells[21]. The $CuInS_2$ film shows a direct optical band gap of 1.45 eV in Fig. 3d, consistent with the reported data[22]. With increasing x in the $CuIn_{1-x}Sn_xS_2$ film, the onset of the absorption coefficient also shifts significantly to NIR range (*i.e.*, ~1.0 eV @ $x = 0.04$), which is similar to the powdered samples. As well known, $CuInS_2$ thin films have been used as light absorber in $CuInS_2$ solar cells with $\eta = 11.4\%$[23]. The drawback is that $CuInS_2$ only absorbs the visible and ultraviolet lights ($\lambda < 825$ nm). The introduction of intermediate band in the $CuIn_{0.96}Sn_{0.04}S_2$ film shows a larger absorption in the solar spectrum (AM 1.5, shown in yellow background in Fig. 3d). Herein, it is promising for the $CuIn_{1-x}Sn_xS_2$ films to combine wide spectrum absorption and high open-circuit voltage in further PV applications.

The underlying reason for Sn doping to extend their absorption spectra needs further investigation. The Sn atoms in the M^{3+} sites have to possess the oxidation state of +3 to balance the charge, similar to Sn_2S_3[24]. The coexisting Sn^{2+} and Sn^{4+} were evidenced by X-ray photoemission spectroscopy (XPS) (Fig. 4a). Two peak structures in the binding energy range from 485 eV to 500 eV observed in $CuGa_{1-x}Sn_xS_2$ are assignable to be Sn $3d_{5/2}$ and Sn $3d_{3/2}$. The asymmetric Sn $3d_{5/2}$ peak was fitted by two peaks with binding energy at 488.3 eV and 487.2 eV, assigned to Sn^{4+}−S and Sn^{2+}−S bonds, respectively[24,25]. Similarly, Sn $3d_{3/2}$ peak was also fitted by two peaks at 496.7 eV and 495.7 eV. Therefore, the partially filled Sn 5*s* states should be located in-between the valance band maximum (VBM)

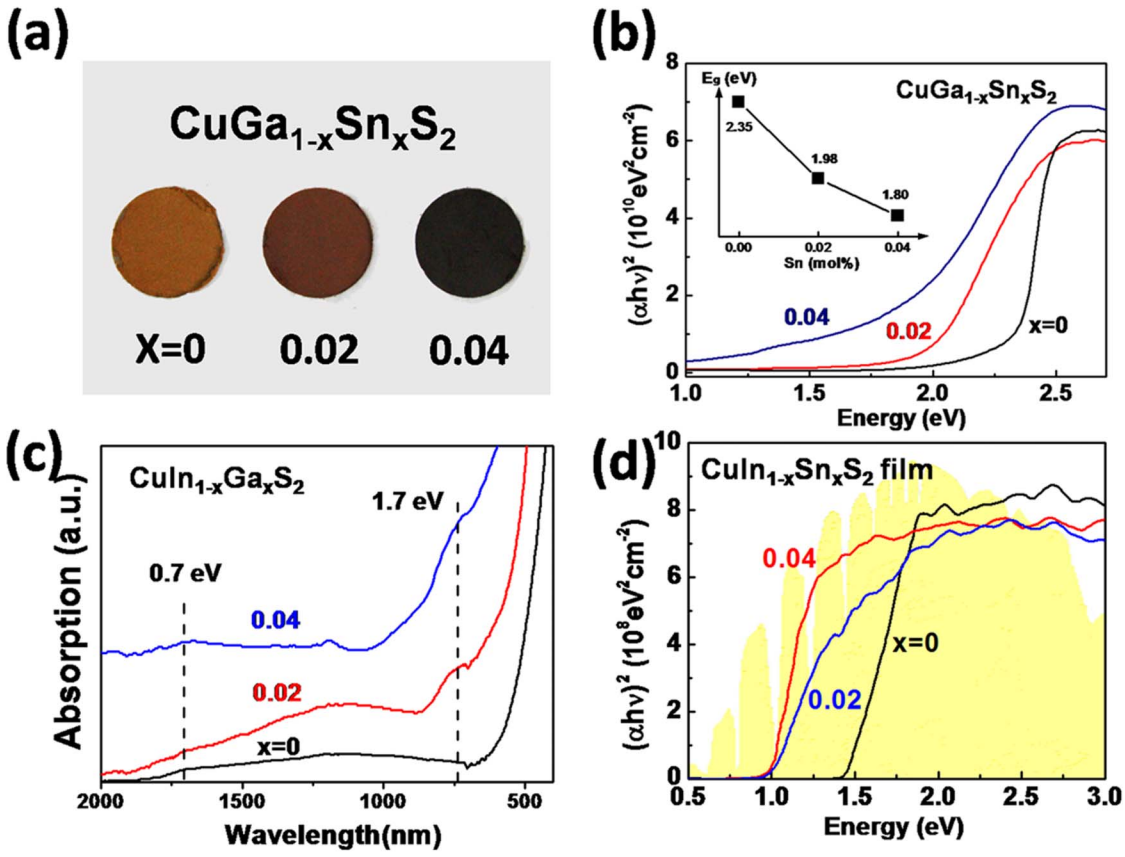

Figure 3 | IBs-induced Wide-spectrum absorption of Sn-doped Chalcopyrites. (a) Photographs of $CuGa_{1-x}Sn_xS_2$ powders. (b) The whole and (c) the partial UV-Vis-NIR diffuse reflectance spectra of $CuGa_{1-x}Sn_xS_2$ powders; inset: the derived band gaps. (d) UV-Vis-NIR diffuse reflectance spectra of $CuIn_{1-x}Sn_xS_2$ films.

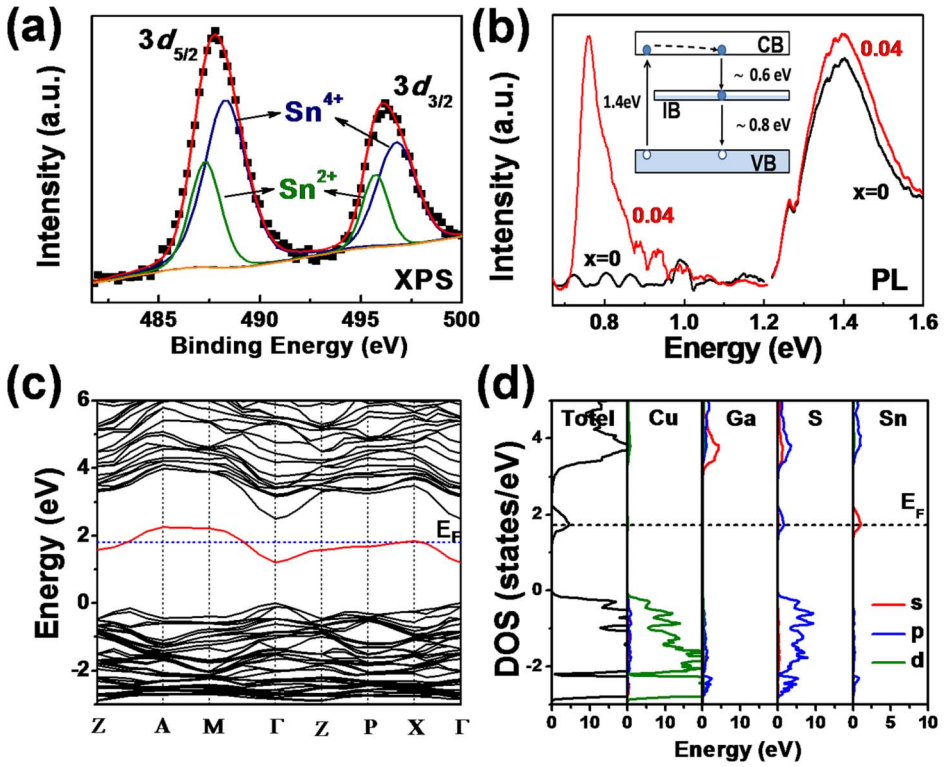

Figure 4 | Analyses of IBs location and band structure. (a) Sn 3*d* XPS spectra of $CuGa_{0.98}Sn_{0.02}S_2$. (b) PL spectra of $CuIn_{1-x}Sn_xS_2$ films; inset: schematic band structure. (c) Band structure of $CuGa_{1-x}Sn_xS_2$; the intermediate band in red. (d) Total and partial DOS of $CuGa_{1-x}Sn_xS_2$.

and the conduction band minimum (CBM) of CuMS_2. In order to monitor the energy states of Sn, the photoluminescence (PL) spectra of the $CuIn_{1-x}Sn_xS_2$ films were performed, as shown in Fig. 4b. The green laser light (λ = 514.5 nm) was employed to excite the films at room temperature. The obvious PL peak centered at ~1.4 eV was observed in all the $CuIn_{1-x}Sn_xS_2$ films, which is identical to the optical absorption edge of $CuInS_2$ (E_g = 1.45 eV), due to the near-bandgap emission. An extra PL peak in the NIR region (~0.78 eV) was also revealed in the Sn-doped film (*e.g.*, x = 0.04). The recombination model of light-excited electron−hole pairs at ~0.78 eV was proposed to occur from IB to VBM, as shown in the inset of Fig. 4b. This is a solid evidence to observe the existence of an intermediate band in Cu$M_{1-x}Sn_xS_2$ ($x \neq 0$). The $CuIn_{0.98}Sn_{0.02}S_2$ also shows an additional PL peak (~0.75 eV) at nearly same position as x = 0.04. The lower peak intensity and narrower full width at half maximum of the peak were observed, which indicate that the distribution of the IB electron states is depended on the doping level of Sn.

Therefore, the E_g reduction in Cu$M_{1-x}Sn_xS_2$, compared with CuMS_2, is due to the intermediate band. According to the theory of quantum leap, the leap probability of electrons from VBM to IB and from IB to CBM is proportional to the density of states (DOS) in IB. Thus, electrons in Sn-doped CuMS_2 are able to be excited from VBM to IB or from IB to CBM, and some photons with $h\nu < E_g$ can be absorbed. However, large Sn doping (>4 mol%) favors solar absorption, but a secondary phase (SnS_2) may occurs.

Discussion

In order to further confirm the intermediate band, the electronic structures of Cu$M_{1-x}Sn_xS_2$ (M = In, Ga) were calculated by first-principles theoretical calculations. The direct transition gaps at Γ (0, 0, 0) are 2.6 eV for CGS and 1.6 eV for CIS (Fig. 4c and S4a), which are consistent with the experimental data (E_g = 2.35 eV for CGS, 1.45 eV for CIS). The direct transition (VBM → CBM) usually leads a high light absorption coefficient due to needing no extra phonon momentum. Surprisingly, the band structure of Sn-doped CuMS_2 is nearly same to the undoped one, except that an intermediate band appears between VBM and CBM. The intermediate band was confirmed by analyzing the DOS of the undoped and the Sn-doped CuMS_2 (Fig. 4d and S4b), which is consistent with the previous calculations[26]. The VBM of CuMS_2 consists of the Cu-3*d* states hybridized with S-3*p*, and the CBM consists of *M*-n*s* (n = 4 for Ga, 5 for In) and S-3*p* states. The partially filled IB mainly contains Sn-5*s* and S-3*p* states, as desired for the IB scheme (Fig. 1b). Hence, Cu$M_{1-x}Sn_xS_2$ has three direct bandgap transitions (VBM → CBM, VBM → IB, IB → CBM) enabling to absorb more photons.

Experimental and theoretical results confirm the existence of intermediate band and much wider spectrum solar response. Such IB materials have not been studied in photocatalysis. Hereby, $CuGa_{1-x}Sn_xS_2$ is selected to verify its IB light absorption and enhanced photocatalysis, as schematized in Fig. 5a. The photocatalytic performance is evaluated by degrading methylene blue (MB) under a xenon light source chopped by two optical high-pass filters (420 nm, 650 nm). The Sn-doped samples show much higher photocatalytic activities than the undoped one under the irradiation of visible-light and NIR spectrum (>420 nm) (Fig. 5b). The respective MB removals over $CuGaS_2$, $CuGa_{0.98}Sn_{0.02}S_2$, and $CuGa_{0.96}Sn_{0.04}S_2$ are 62%, 78%, and 81% after the 90 min illumination. The enhanced photocatalytic activities in the IB samples are apparently due to the wide-spectrum solar response, as derived from the UV-Vis-NIR diffuse reflectance spectra in Fig. 3b. $CuGaS_2$ only absorbs $h\nu_1$ photons (VBM → CBM, >2.35 eV) from the xenon lamp to degrade MB. The IB samples can absorb the extra photons of $h\nu_2$ (IB → CBM, >0.7 eV) and $h\nu_3$ (VBM → IB, >1.7 eV). In order to verify the IB absorption, a 650 nm (1.9 eV) optical high-pass filter was used to cutoff the $>E_g$ photons, and the NIR-light degradations are shown in Fig. 5c. Again, the IB samples are better by comparing the MB removals in 120 min over $CuGa_{1-x}Sn_xS_2$, 10% (x = 0), 24% (x = 0.02), and 34% (x = 0.04), which is attributed to the cascade

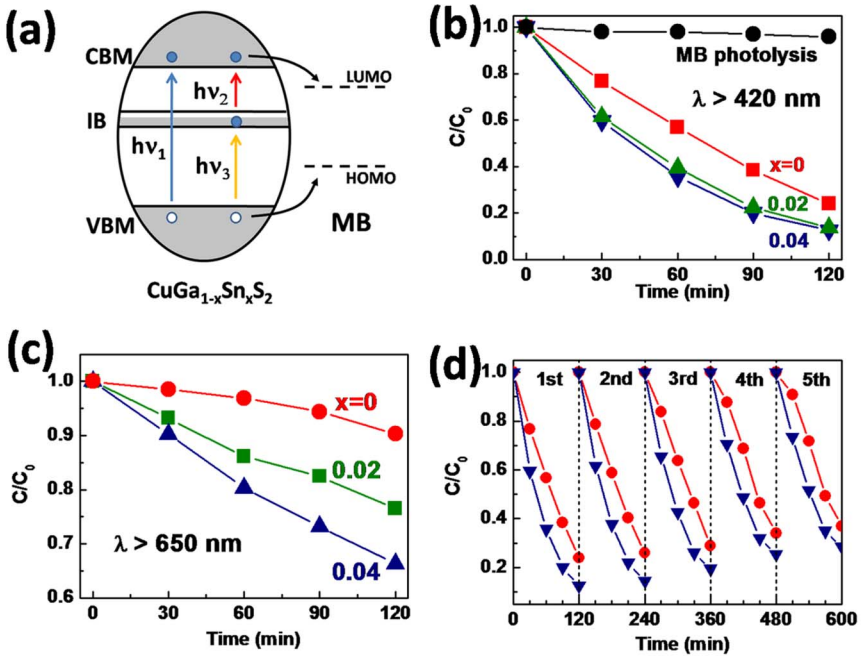

Figure 5 | IBs-induced photocatalysis enhancement. (a) Schematic photocatalysis of $CuGa_{1-x}Sn_xS_2$. Photocatalytic methylene blue degradation under (b) $\lambda > 420$ nm and (c) $\lambda > 650$ nm. (d) Cycling photocatalytic degradations.

absorption of $h\nu_3$ and $h\nu_2$ photons in the Sn-doped $CuGaS_2$. The cycling degradation improvement of $CuGa_{0.96}Sn_{0.04}S_2$ is nearly same in five cycles (Fig. 5d).

Wide-spectrum solar response materials were further verified to improve photovoltaic conversion. The $CuIn_{1-x}Sn_xS_2$ thin films on Mo/SiO_2 substrates were assembled into photoelectrochemical (PEC) cells (Fig. 6a). The electrochemical analysis was conducted in a three-electrode configuration using 0.25 M Na_2S aqueous solution electrolyte. The Mott-Schottky (M-S) plot obtained at the frequency of 1,000 Hz in dark has a negative slope to indicate the *p*-type conduction of $CuInS_2$ (Fig. 6c). The flat-band potential estimated from the extrapolation of the M-S plot is about 0.67 eV relative to

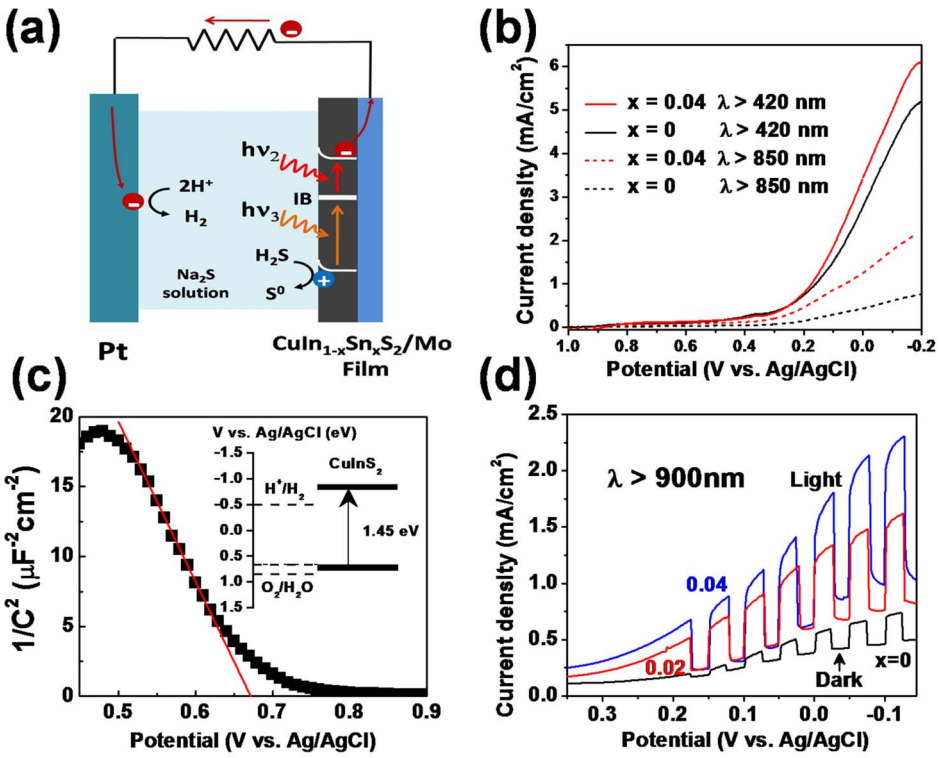

Figure 6 | IBs-induced PEC enhancement. (a) Photoelectrochemical cell with thin-film $CuIn_{1-x}Sn_xS_2$ photoelectrode. (b) Current-potential curves. (c) Mott-Schottky plot of $CuInS_2$ capacitance against potential; inset: CBM and VBM positions. (d) Current-potential curves of $CuIn_{1-x}Sn_xS_2$ under intermittent irradiation.

Ag/AgCl[27]. The alignment of band edge of the $CuInS_2$ film and water redox potential (the insert of Fig. 6c) indicates that the $CuInS_2$ film is available as photocathode for PEC application. Fig. 6b shows linear sweep voltammetry under illumination ($\lambda > 420$ nm), and the photocurrent densities of Sn-doped film are higher than $CuInS_2$ film. At 0 $V_{Ag/AgCl}$, the photocurrent densities were 2.83 mA/cm^2 for $CuInS_2$ and 3.52 mA/cm^2 for $CuIn_{0.96}Sn_{0.04}S_2$. The improvement of photocurrent densities is contributed by the wide-spectrum solar response from the intermediate band effect. In order to get an obvious evidence of this effect, a 900 nm (1.38 eV) optical high-pass filter was used to cutoff the most $>E_g$ photons. Under the NIR light, $CuIn_{0.96}Sn_{0.04}S_2$ has a photocurrent density of is 1.4 mA/cm^2 at 0 $V_{Ag/AgCl}$, much higher than $CuInS_2$ (0.2 mA/cm^2). It was further confirmed by ON/OFF light cycling with the potential swept at 5 mV s^{-1} toward negative potential (Fig. 6d). The remarkable improvement in PEC properties verifies that the intermediate band increases the photocurrent densities by the cascade absorption of $h\nu_3$ (VBM → IB) and $h\nu_2$ (IB → CBM) photons.

In summary, the intermediate band was demonstrated in Sn-doped $CuMS_2$ (M = In, Ga). The uniform nanostructured $CuMS_2$ particles and polycrystalline thin films were synthesized by newly-developed methods. Significant red shifts found in the absorption spectra of $CuM_{1-x}Sn_xS_2$ are caused by the triple absorption bands (VBM → CBM, VBM → IB, IB → CBM), further confirmed by photoluminescence and band structure calculations. Due to wide spectrum response, the enhanced photoelectric conversion revealed the better performance in photocatalysis and photocurrent generation. These results may introduce Sn-doped $CuMS_2$ to be applied in future full-spectrum solar cells.

Methods

Samples preparation. A non-toxic solvent-based process was first developed to prepare nanostructured particles and films of $CuMS_2$ (M = In, Ga). The raw powder of Cu_2S, In_2S_3, and Ga_2S_3 were synthesized in the solid state reactions from the stoichiometric elements of Cu (99.999%, SinoReag), S (99.999%, SinoReag), In (99.999%, SinoReag), and Ga (99.999%, SinoReag) in a sealed evacuated fused silica tube. The nanostructured particles of $CuMS_2$ were harvested from ball-milling the mixtured Cu_2S and M_2S_3 powder with the atomic ratio of Cu : M : S = 1 : 1 : 2 for 24 h. The as-prepared powder were further dispersed in ethanol and further milled for 6 h to obtain the slurry. The precursor thin films of $CuInS_2$ were spin-coated on both SiO_2 and Mo/SiO_2 substrates by using the slurry. All the as-coated films were annealed in H_2S/Ar atmosphere (5 mol% H_2S, 5000 Pa) at 600°C for 15 min. The Sn-doped samples were prepared only by substituting M with Sn from the same procedure described above.

Characterizations. $CuM_{1-x}Sn_xS_2$ powder samples were transferred to a TEM grid (Quantifoil Cu 200 mesh) for these investigations. TEM and STEM elemental mapping were conducted using a JEOL 2100F microscope, operating at 200 kV. Patterns of XRD of the samples were obtained (Bruker D8 FOCUS, at 40 KV and 40 mA) using Cu K_α radiation (λ = 0.15418 nm). The optical absorption spectra of samples were obtained at room temperature by the UV-Vis-NIR spectrometer (Hitachi U4100) equipped with an integrating sphere. The photoluminescence spectra of samples were obtained at room temperature, excited by the green laser light (λ = 514.5 nm) and detected by visible light and NIR (InSb) detectors. XPS experiments were carried out on a RBD upgraded PHI-5000C ESCA system (Perkin Elmer) with Mg K_α radiation ($h\nu$ = 1253.6 eV). Binding energies were calibrated by using the containment carbon (C 1 s = 284.6 eV).

Calculation details. Band structure calculations were performed using the plane-wave projector augmented-wave (PAW) method applying the Heyd-Scuseria-Ernzerhof (HSE) hybrid function[28,29]. We constructed a $\sqrt{2} \times \sqrt{2} \times 1$ supercell which contained 32 atoms and then substituted one M atom by Sn corresponding to the doping content of 12.5%. The cutoff energy of plane wave was chosen at 300 eV.

Photocatalytic and PEC test. The photocatalytic degradation of methylene blue was carried out in a reaction container equipped with an optical system including a 300 W xenon lamp and optical high-pass filters with the different cutoff wavelengths. The transparency spectra of the filters are shown in Fig. S3 of Supporting Information. The volume of the initial 10 mg/L MB solution is 200 ml, and the catalyst powder are 100 mg. Light illumination is conducted after the suspension is stirred in the dark for 30 min to reach the adsorption–desorption equilibrium of organic dye on catalyst surface. During irradiation, about 3 ml suspension is continually taken from the reaction cell at given time intervals for subsequent MB concentration analysis after centrifuging. PEC measurements were performed in a typical three-electrode potentiostat system (Parstat 2773), in which the $CuIn_{1-x}Sn_xS_2$ film on Mo/SiO_2 substrate, a Pt wire, and an Ag/AgCl electrode were used as the working, counter, and reference electrodes, respectively. 0.25 M Na_2S aqueous solution was used as the supporting electrolyte to maintain the stability of films. A solar simulator (AM 1.5) with a power of 100 mW/cm^2 was used as the illumination source. Photocurrent ON/OFF cycles were measured using the same electrochemical workstation coupled with a mechanical chopper.

1. Shockley, W. & Queisser, H. J. Detailed Balance Limit of Efficiency of p-n Junction Solar Cells. *J. Appl. Phys.* **32**, 510–519 (1961).
2. Green, M. A., Emery, K., Hishikawa, Y. & Warta, W. Solar cell efficiency tables (Version 32). *Prog. Photovoltaics Res. Appl.* **16**, 435–440 (2008).
3. Luque, A., Martí, A. & Stanley, C. Understanding intermediate-band solar cells. *Nat Photon* **6**, 146–152 (2012).
4. López, N., Reichertz, L. A., Yu, K. M., Campman, K. & Walukiewicz, W. Engineering the Electronic Band Structure for Multiband Solar Cells. *Phys. Rev. Lett.* **106**, 028701–4 (2011).
5. Jackson, P., Hariskos, D., Lotter, E., Paetel, S., Wuerz, R., Menner, R., Wischmann, W. & Powalla, M. New world record efficiency for Cu(In,Ga)Se_2 thin-film solar cells beyond 20%. *Prog. Photovoltaics Res. Appl.* **19**, 894–897 (2011).
6. Siebentritt, S. Wide gap chalcopyrites: material properties and solar cells. *Thin Solid Films* **403–404**, 1–8 (2002).
7. Palacios, P., Sánchez, K., Conesa, J., Fernández, J. & Wahnón, P. Theoretical modelling of intermediate band solar cell materials based on metal-doped chalcopyrite compounds. *Thin Solid Films* **515**, 6280–6284 (2007).
8. Aguilera, I., Palacios, P. & Wahnón, P. Enhancement of optical absorption in Ga-chalcopyrite-based intermediate-band materials for high efficiency solar cells. *Sol. Energy Mater. Sol. Cells* **94**, 1903–1906 (2010).
9. Palacios, P., Sánchez, K., Conesa, J. C. & Wahnón, P. First principles calculation of isolated intermediate bands formation in a transition metal-doped chalcopyrite-type semiconductor. *Phys. Stat. Sol. A* **203**, 1395–1401 (2006).
10. Marrón, D. F., Martí, A. & Luque, A. Thin-film intermediate band photovoltaics: advanced concepts for chalcopyrite solar cells. *Phys. Stat. Sol. A* **206**, 1021–1025 (2009).
11. Tablero, C. & Fuertes Marrón, D. Analysis of the Electronic Structure of Modified $CuGaS_2$ with Selected Substitutional Impurities: Prospects for Intermediate-Band Thin-Film Solar Cells Based on Cu-Containing Chalcopyrites. *J. Phys. Chem. C* **114**, 2756–2763 (2010).
12. Marsen, B., Steinkopf, L., Singh, A., Wilhelm, H., Lauermann, I., Unold, T., Scheer, R. & Schock, H. W. Effects of Ti-incorporation in $CuInSe_2$ solar cells. *Sol. Energy Mater. Sol. Cells* **94**, 1730–1733 (2010).
13. Marsen, B., Klemz, S., Unold, T. & Schock, H. W. Investigation of the Sub-Bandgap Photoresponse in $CuGaS_2$:Fe for Intermediate Band Solar Cells. *Prog. Photovoltaics Res. Appl.* **20**, 625–629 (2012).
14. Abrahams, S. C. & Bernstein, J. L. Piezoelectric nonlinear optic $CuGaS_2$ and $CuInS_2$ crystal structure: Sublattice distortion in $A^IB^{III}C_2^{VI}$ and $A^{II}B^{IV}C_2^{V}$ type chalcopyrites. *J. Chem. Phys.* **59**, 5415–5422 (1973).
15. Fang, A. H., Huang, F. Q., Xie, X. M. & Jiang, M. H. Low-Temperature Rapid Synthesis and Superconductivity of Fe-Based Oxypnictide Superconductors. *J. Am. Chem. Soc.* **132**, 3260–3261 (2010).
16. Yang, C. Y., Wang, Y. M., Li, S. T., Wan, D. Y. & Huang, F. Q. $CuSbSe_2$-assisted sintering of $CuInSe_2$ at low temperature. *J. Mater. Sci.* **47**, 7085–7089 (2012).
17. Surek, T. Crystal growth and materials research in photovoltaics: progress and challenges. *J. Cryst. Growth* **275**, 292–304 (2005).
18. Palm, J., Probst, V., Stetter, W., Toelle, R., Visbeck, S., Calwer, H., Niesen, T., Vogt, H., Hernández, O., Wendl, M. & Karg, F. H. CIGSSe thin film PV modules: from fundamental investigations to advanced performance and stability. *Thin Solid Films* **451–452**, 544–551 (2004).
19. Tanaka, K., Moritake, N. & Uchiki, H. Preparation of thin films by sulfurizing sol–gel deposited precursors. *Sol. Energy Mater. Sol. Cells* **91**, 1199–1201 (2007).
20. Panthani, M. G., Akhavan, V., Goodfellow, B., Schmidtke, J. P., Dunn, L., Dodabalapur, A., Barbara, P. F. & Korgel, B. A. Synthesis of $CuInS_2$, $CuInSe_2$, and Cu(In_xGa_{1-x})Se_2 (CIGS) Nanocrystal "Inks" for Printable Photovoltaics. *J. Am. Chem. Soc.* **130**, 16770–16777 (2008).
21. Zhu, X. L., Zhou, Z., Wang, Y. M., Zhang, L., Li, A. M. & Huang, F. Q. Determining factor of $MoSe_2$ formation in Cu(In,Ga)Se_2 solar Cells. *Sol. Energy Mater. Sol. Cells* **101**, 57–61 (2012).
22. Antony, A., Asha, A. S., Yoosuf, R., Manoj, R. & Jayaraj, M. K. Growth of $CuInS_2$ thin films by sulphurisation of Cu–In alloys. *Sol. Energy Mater. Sol. Cells* **81**, 407–417 (2004).
23. Braunger, D., Hariskos, D., Walter, T. & Schock, H. W. An 11.4% efficient polycrystalline thin film solar cell based on $CuInS_2$ with a Cd-free buffer layer. *Sol. Energy Mater. Sol. Cells* **40**, 97–102 (1996).
24. Cruz, M., Morales, J., Espinos, J. P. & Sanz, J. XRD, XPS and 119 Sn NMR study of tin sulfides obtained by using chemical vapor transport methods. *J. Solid State Chem.* **175**, 359–365 (2003).
25. Morgan, W. E. & Van Wazer, J. R. Binding energy shifts in the x-ray photoelectron spectra of a series of related Group IVa compounds. *J. Phys. Chem.* **77**, 964–969 (1973).

26. Luque, A. & Martí, A. Increasing the Efficiency of Ideal Solar Cells by Photon Induced Transitions at Intermediate Levels. *Phys. Rev. Lett.* **78**, 5014–5017 (1997).
27. Li, T. L. & Teng, H. Solution synthesis of high-quality $CuInS_2$ quantum dots as sensitizers for TiO_2 photoelectrodes. *J. Mater. Chem.* **20**, 3656–3664 (2010).
28. Blöchl, P. E. Projector augmented-wave method. *Phys. Rev. B* **50**, 17953–17979 (1994).
29. Heyd, J., Scuseria, G. E. & Ernzerhof, M. Hybrid functionals based on a screened Coulomb potential. *J. Chem. Phys.* **118**, 8207–8215 (2003).
30. Yu, K. M., Walukiewicz, W., Wu, J., Shan, W., Beeman, J. W., Scarpulla, M. A., Dubon, O. D., & Becla, P. Diluted II-VI oxide semiconductors with multiple band gaps. *Phys. Rev. Lett.* **91**, 246403–246404 (2003).
31. Lucena, R., Aguilera, I., Palacios, P., Wahnon, P. & Conesa, J. C. Synthesis and spectral properties of nanocrystalline V-Substituted In_2S_3: A novel material for more efficient use of solar radiation. *Chem. Mater.* **20**, 5125–5127 (2008).

Acknowledgment

The authors thank Prof. I-Wei Chen at the University of Pennsylvania for fruitful discussions and insightful suggestions. Financial support was from National 863 Program of China (Grant No. 2011AA050505), NSF of China (Grant Nos. 91122034, 51125006, 51121064, 51102263), and Innovation Program of the CAS (Grant No. KJCX2-EW-W11).

Author contributions

C.Y.Y. designed the experiments, synthesized materials, conducted all the tests and wrote the manuscript. Q.M.S. designed the experiments and processed synthesis of thin films. D.Y.W. and Y.M.W. designed and conducted PEC tests. F.Q.H. and J.H.L. supervised the overall project, designed the experiments, and wrote the manuscript.

Additional information

Supplementary information accompanies this paper at http://www.nature.com/scientificreports

Competing financial interests: The authors declare no competing financial interests.

How to cite this article: Yang, C. *et al.* Observation of an Intermediate Band in Sn-doped Chalcopyrites with Wide-spectrum Solar Response. *Sci. Rep.* **3**, 1286; DOI:10.1038/srep01286 (2013).